jaa Just accepted article

EuroIntervention

Title: Identification of the type of stent with three-dimensional optical coherence tomography: the SPQR study.

Authors: Carlos Cortés, M.D, PhD; Miao Chu, MS; Michele Schincariol, M.D; Miguel Ángel Martínez-Hervás-Alonso, M.D; Bernd Reisbeck, M.D; Ruiyan Zhang, M.D, PhD; Yoshinobu Murasato, M.D, PhD; Shao-Liang Chen, M.D, PhD; Francesco Lavarra, M.D; Shengxian Tu, PhD; Sigmund Silber, M.D, FESC, FACC; Juan Luis Gutiérrez-Chico, M.D, PhD, FESC, FACC

DOI: 10.4244/EIJ-D-20-00598

Citation: Cortés C, Chu M, Schincariol M, Martínez-Hervás-Alonso MA, Reisbeck B, Zhang R, Murasato Y, Chen S, Lavarra F, Tu S, Silber S, Gutiérrez-Chico JL. Identification of the type of stent with three-dimensional optical coherence tomography: the SPQR study. *EuroIntervention* 2020; Jaa-842, 2020, doi: 10.4244/EIJ-D-20-00598

Manuscript submission date: 12 May 2020

Revisions received: 11 August 2020

Accepted date: 09 September 2020

Online publication date: 15 September 2020

Identification of the type of stent with three-dimensional optical coherence tomography: the SPQR study

Carlos Cortés, MD, PhD[1,2*]; Miao Chu, MS[3,4*]; Michele Schincariol, MD[5]; Miguel Ángel Martínez-Hervás-Alonso, MD[3]; Bernd Reisbeck, MD[3]; Ruiyan Zhang, MD, PhD[6,7]; Yoshinobu Murasato, MD, PhD[8]; Shao-Liang Chen, MD, PhD[9]; Francesco Lavarra, MD[10]; Shengxian Tu, PhD[4]; Sigmund Silber, MD, FESC, FACC[11]; Juan Luis Gutiérrez-Chico, MD, PhD, FESC, FACC[1,3,12]

1.- Klinikum Frankfurt (Oder), Germany
2.- San Pedro Hospital, Logroño, Spain
3.- Cardiology Department, Campo de Gibraltar Health Trust, Algeciras, Spain
4.- Med-X Research Institute, School of Biomedical Engineering, Shanghai Jiao Tong University, Shanghai, China
5.- Klinikum Fürth, Cardiology Department, Germany
6.- Ruijin Hospital, Shanghai, China
7.- Medical University, Shanghai Jiao Tong University, Shanghai, China
8.- Kyushu Medical Center, Fukuoka, Japan
9.- Nanjing First Hospital, Nanjing, China
10.- Jilin Heart Hospital, Changchun, China
11.- Cardiology Practice, Munich, Germany
12.- DRK Klinikum Westend, Berlin, Germany

* These authors have equally contributed.

Short running title: Stent pattern recognition with 3D-OCT

Keywords: optical coherence tomography; bare-metal stent; drug-eluting stent; bioresorbable scaffolds

Conflict of interest / funding: The authors have no conflict of interests to disclose.

Corresponding author:
Prof. Juan Luis Gutiérrez-Chico, MD, PhD, FESC, FACC
Head of the Cardiology Department
Hospital Punta de Europa
Crtra. Getares s/n
11207 – Algeciras (Cádiz), Spain
juanluis.gutierrezchico@ictra.es

Abstract

Background: The ability of optical coherence tomography (OCT) to identify specific types of stent has never been systematically studied.

Methods and results: A series of 212 consecutive patients with OCT from six international centres were retrospectively screened, finding 294 metallic stents or scaffolds in 146 patients. The sample was analysed by two blinded operators, applying a dedicated protocol in 4 steps to identify the type of stent: 1) 3D and automatic strut detection (ASD), 2) 3D tissue view, 3) Longitudinal view with ASD, 4) Mode "stent only" and ASD. The protocol correctly identified 285 stents (96.9%, kappa 0.965), with excellent interobserver agreement (kappa 0.988). The performance tended to be better in recently implanted stents (kappa 0.993) than in stents implanted ≥3 months before (kappa 0.915), and in pullback speed 18mm/s as compared with 36 mm/s (kappa 0.969 vs. 0.940, respectively).

Conclusion: The type of stent platform can be accurately identified in OCT by trained analysts following a dedicated protocol, combining 3D-OCT, ASD and longitudinal view. This might be clinically helpful in scenarios of device failure and for the quantification of apposition. The blinding of analysts in OCT studies should be revisited.

Condensed abstract

A series of 294 metallic stents in 146 consecutive patients with OCT from six international centres was retrospectively analysed by two blinded operators, applying a dedicated protocol in 4 steps to identify the type of stent implanted, combining 3D-OCT, automatic strut detection and longitudinal view. The protocol correctly identified 285 stents (96.9%, kappa 0.965), with excellent interobserver agreement (kappa 0.988). The type of stent platform can be accurately identified in OCT by trained analysts. This might be clinically helpful in scenarios of device failure and for the quantification of apposition. The blinding of analysts in OCT studies should be revisited.

List of abbreviations

3D-OCT: Three-dimensional optical coherence tomography

ASD: Automatic strut detection

BRS: Bioresorbable scaffold

ISR: In-stent restenosis

DES: Drug-eluting stent

LAD: Left anterior descending

NIR: Near-infrared

NURD: Non-uniform rotational distortion

OCT: Optical coherence tomography

RCA: Right coronary artery

Introduction

Three-dimensional (3D) optical coherence tomography (OCT) has proven its usefulness for the treatment of complex bifurcations, to assist the wire recrossing through the right stent cell[1] or to assess the structural integrity of bioresorbable scaffolds (BRS)[2, 3]. The ability of 3D-OCT to identify the type of stent implanted, in case this information were unknown and relevant, has been suggested in some reports[4], but its accuracy for this indication has never been systematically studied. The identification of the stent is clinically and scientifically relevant, because it might provide the operator with meaningful information to make tailored decisions in challenging cases, particularly in the setting of device failure[4, 5], but also for accurate quantification of apposition[6, 7] or because it might jeopardise the blinding of the analysts in randomised clinical trials involving OCT quantification[6-8].

The SPQR (Stent Pattern Qualitative Recognition) study appraises the feasibility and accuracy of identifying the type of stent previously implanted by means of 3D-OCT, strut automatic detection and longitudinal OCT reconstruction.

Methods

Consecutive patients undergoing OCT of a coronary artery previously treated with implantation of a metallic stent, durable or bioresorbable, in any of the participating centres (Klinikum Frankfurt Oder, Germany; DRK Klinikum Westend, Berlin, Germany and Campo de Gibraltar Health Trust, Algeciras, Spain) between 01-03-2016 and 01-08-2019 were retrospectively included into the study. Exclusion criteria were 1) previous treatment of the target vessel with non-metallic bioresorbable scaffolds alone; 2) overlapping stents or multiple stent layers leaving <5mm monolayer segment; 3) poor OCT quality due to non-uniform rotational distortion (NURD), incomplete purge of the optical catheter, suboptimal vessel flushing or other artefacts[9] and 4) severe stent distortion due to longitudinal stress or collapse of the lumen, leaving <5mm of stent structurally preserved and suitable for analysis. All OCT studies were acquired with a Dragonfly™ catheter and an ILUMIEN OPTIS system (Abbott, St Paul, Minnesota, USA), at rotation speed of 180 Hz and pullback speed of 18 mm/s or 36 mm/s, resulting in longitudinal resolutions of 0.1 and 0.2 mm, respectively. The operators used non-occlusive technique[10] and automatic contrast injection, calculating the contrast volume with a formula to optimise quality with minimal amount of dye[11]. The sample was completed with selected cases from three Asian centres, containing paradigmatic examples of some stent types not found in the European sample. These selected cases were intercalated into the sample at random positions for analysis.

Clinical information about patients, procedures and type of stents previously implanted was retrospectively collected from clinical recordings in each centre. Target stents were classified as recently (<3 months) or late implanted (≥3 months).

The study complied with the principles of good clinical practice and with the Declaration of Helsinki for investigation in human beings. The study protocol was approved by the institutional review boards of the participating hospitals.

Nomenclature for description of the stent platforms

Although most technical studies describe the stent platforms in terms of peaks or valleys depending on the angle between the longitudinal connector and the hoops (obtuse or acute, respectively)[12-14], this terminology was proved inappropriate for the current analysis, because it created unsolvable ambiguities. A specifically dedicated nomenclature was defined.

Two fundamental components were considered: sinusoidal hoops and longitudinal connectors. Peaks and valleys were defined in the sinusoidal hoops as hinge points with the vertex pointing to the distal and proximal parts of the vessel, respectively (figure 1). The struts connecting peaks and valleys were dubbed slopes. Hoops were considered in-phase if peaks faced peaks in adjacent hoops, out-of-phase if peaks faced valleys or offset if peaks faced slopes. Longitudinal connectors were defined according to the points of the hoop that they connected (peak-to-peak, peak-to-valley, valley-to-valley or connecting the slopes, figure 2) and according to unique morphological features of their design (crenelated, S-shaped, step-shaped, etc.).

Patterns of the different stent platforms and OCT analysis.

Supplementary table 1 and figure 3 summarise the characteristics of the stent platforms in this study, according to the nomenclature explained above.

OCT raw data were evaluated by two independent blinded analysts, using an Ilumien Optis E.5 workstation (Abbott, St Paul, Minnesota, USA). After identification of the stented segment and the corresponding analysable monolayer (in case of overlapping), the analysts underwent the following protocol to identify the pattern of the stent platform, rotating the image at discretion: 1) 3D view with automatic strut detection; 2) 3D tissue view, without automatic strut detection; 3) longitudinal view with automatic strut detection; 4) 3D view in mode “stent

only" (figure 4). The analysts recorded at which steps of the protocol the type of stent platform could be recognised. After completing the 4 steps of the protocol, the analyst had to identify the type of stent previously implanted as one of the 20 categories defined in supplementary table 1 and figure 3, or label the case as unrecognisable.

Statistical analysis.

Descriptive statistics of continuous variables were reported as mean ± SD if they followed a Gaussian distribution or as median (quartiles) if differently distributed, while those of categorical variables were presented as counts (percentages). The agreement between analyst 1 and the type of stent platform previously implanted was reported as kappa coefficient and stratified according to the timing of stent implant (recently vs. late implanted) and pullback speed (18 vs. 36 mm/s). Interobserver reproducibility was reported as kappa coefficient. Efficiency analysis of the steps was reported as % of stents recognised in each step. All analysis were performed with IBM SPSS 24.0 software package (SPSS Inc., Chicago, Illinois).

Results

A total of 193 patients underwent OCT studies in the enrolling centres during the study period. The sample was completed with 19 selected patients from Asian centres with paradigmatic examples of specific stent types. Sixty-six patients (68 studies) were excluded: 40 because no stent was imaged in the OCT study (58.8%), 22 because only non-metallic BRS was implanted in the intervention (32.4%), 3 due to suboptimal vessel flushing (4.4%), 2 due to severe stent distortion (2.9%) and 1 due to NURD (1.5%). During the analysis 21 stents were excluded due to multilayer (8), overlap with <5mm of monolayer (8), suboptimal vessel flushing (3), incomplete purge of the optical catheter (1) or NURD (1). A total of 146 patients,

155 procedures, 179 lesions, 196 pullbacks and 294 stents were finally analysed according to the protocol (figure 5).

Descriptive statistics of the sample.

Tables 1 and 2 present the descriptive statistics of the sample. Different types of stent were analysed in the study: ML Rx Pixel, ML Zeta, Vision and Xience (Abbott Vascular, Santa Clara, CA); Driver, Resolute Integrity and Resolute Onyx (Medtronic, Santa Rosa, CA); Orsiro and Magmaris (Biotronik AG, Bülach, CH); Biomatrix and Biofreedom (Biosensors International, Morges, CH); Coroflex (B. Braun, Melsungen DE); Cypher select (Cordis, Santa Clara, CA); Taxus Express, Taxus Liberté and Promus Element (Boston Scientific, Marlborough, MA); Nobori (Terumo, Tokyo, JP); Firebird and Firehawk (Microport, Shanghai, CN); Alex Plus and Bioss-Lim C (Balton, Warsaw, PL); Biodivysio (Biocompatibles Ltd, Farnham, UK) and Costar (Conor MedSystems, Menlo Park, CA)[15]. One hundred seven stents (36.4%) were implanted more than 3 months prior to the OCT study and 62 (21.1%) presented in-stent restenosis (ISR) as anatomic substrate for the clinical symptoms. All ISR stents but 3 were implanted ≥3 months before. Most studies (77.2%) were acquired at a pullback speed of 18 mm/s.

Feasibility, agreement and reproducibility.

Eight cases (2.7%) were deemed unrecognisable by the main analyst and in one additional case (0.3%) the identification was wrong. Five unrecognisable cases and the misclassified stent corresponded to ISR. All other cases were correctly identified, resulting in a feasibility of 96.9% , kappa 0.965 (95% CI: 0.943 – 0.987; p <0.0001). Both analysts agreed in all but 3 cases (1.0%), corresponding to a kappa 0.988 (95% CI: 0.974 – 1.00, p<0.0001) for the interobserver agreement (table 3).

Table 3 presents the results of agreement stratified by timing of stent implant and by pullback speed. The agreement tended to be worse in late implanted stents (kappa 0.915; 95% CI: 0.860 – 0.970), in cases of ISR (kappa 0.889; 95% CI: 0.807 – 0.971) and if the pullback was acquired at 36 mm/s (kappa 0.940; 95% CI: 0.875 – 1.000). Conversely, recently implanted stents were accurately identified in all but 1 case, thus presenting a kappa coefficient close to perfect agreement (kappa 0.993; 95% CI: 0.981 – 1.000).

Efficiency of the protocol steps.

In recently implanted stents, step 2 (3D tissue view) was the most effective (100% identification at 18 mm/s; 97.7% at 36 mm/s; table 4, figure 6). In 14 cases (7.5%) the stent could be recognised only in step 2 (table 4, figure 7).

Conversely, in late implanted stents the most efficient step was the 3rd one (longitudinal view): 90.4 % identification at 18 mm/s; 91.7% at 36 mm/s (table 4, figure 6). The combination of steps played a critical role in late implanted stents, as 5 cases (4.7%) were only identifiable in step 3 and 3 cases (2.8%) only identifiable in step 2 (table 4, figure 7).

Discussion

The current study proves that the type of stent previously implanted in a coronary artery can be accurately identified by OCT, combining 3D reconstruction, automatic strut detection and longitudinal view. An operative description of the different stent platforms, based on simple differential features of their design, together with a systematic stepwise protocol, resulted in accurate pattern recognition by trained analysts, with excellent feasibility and reproducibility.

The identification of the specific type of stent implanted might be important in different clinical scenarios, mostly related to stent failure, as patients often undergo the intervention before the whole relevant information about previous procedures can be reliably collected. As

different types of stents are associated with different mechanisms of thrombosis, it is critical to understand the pathophysiology underneath each case to implement the most appropriate treatment. First-generation drug-eluting stents (DES) were associated with hypersensitivity reactions resulting in inflammation and thrombosis[16, 17], while 2nd-generation DES were not. In a recently-published case of very-late DES thrombosis, 3D-OCT enabled the identification of a 1st-generation DES and a 2nd-generation DES in the same vessel: the thrombosis was depending on the latter due to severe structural distortion[4]. The treatment could be then directed to the restoration of normal biomechanics, with no concerns about implanting more metal or polymer. The therapeutic plan would have been different if the thrombosis were dependant on the 1st-generation DES[4]. Likewise, the most solid evidence to date about the treatment of in-stent restenosis (ISR) points out that switching to a different type of DES might be better than insisting on the same DES type[5]. However the information about the restenosed DES is sometimes missing, due to incomplete reports or patients treated in another centre. A refined interventional cardiologist must know which type of stent is treating and the mechanisms that most likely triggered the stent failure. If this information is missing, it can be elucidated with standard OCT.

The quantification of apposition requires the subtraction of the specific strut thickness from the malapposition distance[6, 7]. This method can be inaccurate if the type of stent is unknown or if it must remain unknown, in case of randomised studies. The ability of a trained analyst to identify the type of stent should be considered in clinical trials with OCT endpoints, wherein the analyst must be blind to the stent adjudication. The quantification software should not allow the analyst to get 3D or longitudinal views with strut detection, because the type of stent would be then unravelled. Artificial intelligence might automate the process of stent recognition for assessment of malapposition in a near future, as deep convolutional networks are already performing automatic strut detection taking the stent pattern into account[18].

Our results highlight the importance of combining the different steps of the protocol, particularly in late implanted stents. Supplementary table 2 summarises the characteristics and technical requirements of each step. All steps except 3D tissue view depend on automatic strut detection, whilst steps 1 and 4 require post-processing of the detected struts. The most efficient steps are independent of these technical tools. Post-processing may be helpful in filling the gaps between struts, rendering an accurate stent structure, but it can be misleading in complex stent designs. In recently implanted stents, 3D tissue view (i.e. the sheer OCT image) is the most efficient step, just depending on the longitunal resolution of the pullback. Late implanted stents, however, are often deeply buried in neointima and leave no recognisable relief on the intimal surface, so 3D tissue view can be outperformed by longitudinal view, depending on the longitudinal resolution and accurate strut detection.

Limitations:

This is a retrospective offline analysis performed on standard real-world OCT pullbacks by trained analysts. The performance of the protocol applied by local operators onsite should be prospectively confirmed.

Some DES share the same stent platform as their corresponding bare-metal stents or even as other DES. In these cases, the identification of the platform does not permit to infer the exact type, but it reduces substantially the level of uncertainty. Complementary information about local trends on stents availability might often solve the potential ambiguity.

The sample of stents in the study reflects local practice and availability in the study centres. Some platforms were described, but no paradigmatic example of them could be found. The description of these platforms is however kept in the manuscript for didactic purposes. Likewise, some stent platforms excluded from the description might be however commonly used in other centres, requiring local adaptations of the protocol.

Conclusion

The stent platform implanted in a coronary artery can be accurately identified in OCT by trained analysts following a dedicated protocol, combining 3D-OCT, automatic strut detection and longitudinal view. This might be clinically helpful in scenarios of device failure and for the quantification of apposition. The blinding of analysts in OCT studies should be revisited.

Impact on daily practice

The ability of OCT to identify the type of stent previously implanted can be potentially useful in cases of stent failure, in which specific information is often missing or misleading at the time of the intervention. The quantification of apposition could be automated and facilitated by incorporating convolutional models for automatic stent identification in future updates of the software. Finally, the blinding of OCT studies must be revisited after proving that a trained analyst can efficiently identify the type of stent aided by 3D reconstruction or by longitudinal view.

Acknowledgements

To Lili Liu (Ruijin Hospital, Shanghai), Jing Kan (Nanjing Heart Centre) and Qi Zhou (Microport) for their technical assistance.

Reference List

(1) Okamura T, Nagoshi R, Fujimura T, Murasato Y, Yamawaki M, Ono S, Serikawa T, Hikichi Y, Norita H, Nakao F, Sakamoto T, Shinke T, Shite J. Impact of guidewire recrossing point into stent jailed side branch for optimal kissing balloon dilatation: core lab 3D optical coherence tomography analysis. *EuroIntervention* 2018 February 2;13(15):e1785-e1793.

(2) Gogas BD, van Geuns RJ, Farooq V, Regar E, Heo JH, Ligthart J, Serruys PW. Three-dimensional reconstruction of the post-dilated ABSORB everolimus-eluting bioresorbable vascular scaffold in a true bifurcation lesion for flow restoration. *JACC Cardiovasc Interv* 2011 October;4(10):1149-50.

(3) Farooq V, Gogas BD, Okamura T, Heo JH, Magro M, Gomez-Lara J, Onuma Y, Radu MD, Brugaletta S, van BG, van Geuns RJ, Garcia-Garcia HM, Serruys PW. Three-dimensional optical frequency domain imaging in conventional percutaneous coronary intervention: the potential for clinical application. *Eur Heart J* 2013 March;34(12):875-85.

(4) Jaguszewski MJ, Cortes C, Daucher H, Schincariol M, Halejcio M, Besuch P, Gutierrez-Chico JL. Very late stent thrombosis in everolimus-eluting stent with predisposing mechanical factors: Differential features. *Cardiol J* 2017;24(4):345-9.

(5) Alfonso F, Perez-Vizcayno MJ, Dutary J, Zueco J, Cequier A, Garcia-Touchard A, Marti V, Lozano I, Angel J, Hernandez JM, Lopez-Minguez JR, Melgares R, Moreno R, Seidelberger B, Fernandez C, Hernandez R. Implantation of a drug-eluting stent with a different drug (switch strategy) in patients with drug-eluting stent restenosis. Results from a prospective multicenter study (RIBS III [Restenosis Intra-Stent: Balloon Angioplasty Versus Drug-Eluting Stent]). *JACC Cardiovasc Interv* 2012 July;5(7):728-37.

(6) Gutierrez-Chico JL, van Geuns RJ, Regar E, van der Giessen WJ, Kelbaek H, Saunamaki K, Escaned J, Gonzalo N, Di MC, Borgia F, Nuesch E, Garcia-Garcia HM, Silber S, Windecker S, Serruys PW. Tissue coverage of a hydrophilic polymer-coated zotarolimus-eluting stent vs. a fluoropolymer-coated everolimus-eluting stent at 13-month follow-up: an optical coherence tomography substudy from the RESOLUTE All Comers trial. *Eur Heart J* 2011 June 9;32:2454-63.

(7) Gutiérrez-Chico JL, Regar E, Nüesch E, Okamura T, Wykrzykowska J, di Mario C, Windecker S, van Es GA, Gobbens P, Jüni P, Serruys PW. Delayed Coverage in Malapposed and Side-Branch Struts With Respect to Well-Apposed Struts in Drug-Eluting Stents. *Circulation* 2011 August 2;124(5):612-23.

(8) Guagliumi G, Costa MA, Sirbu V, Musumeci G, Bezerra HG, Suzuki N, Matiashvili A, Lortkipanidze N, Mihalcsik L, Trivisonno A, Valsecchi O, Mintz GS, Dressler O, Parise H, Maehara A, Cristea E, Lansky AJ, Mehran R, Stone GW. Strut Coverage and Late Malapposition With Paclitaxel-Eluting Stents Compared With Bare Metal Stents in Acute Myocardial Infarction: Optical Coherence Tomography Substudy of the

Harmonizing Outcomes With Revascularization and Stents in Acute Myocardial Infarction (HORIZONS-AMI) Trial. *Circulation* 2011 January 25;123(3):274-81.

(9) Tearney GJ, Regar E, Akasaka T, Adriaenssens T, Barlis P, Bezerra HG, Bouma B, Bruining N, Cho JM, Chowdhary S, Costa MA, de SR, Dijkstra J, Di MC, Dudeck D, Falk E, Feldman MD, Fitzgerald P, Garcia H, Gonzalo N, Granada JF, Guagliumi G, Holm NR, Honda Y, Ikeno F, Kawasaki M, Kochman J, Koltowski L, Kubo T, Kume T, Kyono H, Lam CC, Lamouche G, Lee DP, Leon MB, Maehara A, Manfrini O, Mintz GS, Mizuno K, Morel MA, Nadkarni S, Okura H, Otake H, Pietrasik A, Prati F, Raber L, Radu MD, Rieber J, Riga M, Rollins A, Rosenberg M, Sirbu V, Serruys PW, Shimada K, Shinke T, Shite J, Siegel E, Sonada S, Suter M, Takarada S, Tanaka A, Terashima M, Troels T, Uemura S, Ughi GJ, van Beusekom HM, van der Steen AF, Van Es GA, van SG, Virmani R, Waxman S, Weissman NJ, Weisz G. Consensus standards for acquisition, measurement, and reporting of intravascular optical coherence tomography studies: a report from the International Working Group for Intravascular Optical Coherence Tomography Standardization and Validation. *J Am Coll Cardiol* 2012 March 20;59(12):1058-72.

(10) Prati F, Cera M, Ramazzotti V, Imola F, Giudice R, Albertucci M. Safety and feasibility of a new non-occlusive technique for facilitated intracoronary optical coherence tomography (OCT) acquisition in various clinical and anatomical scenarios. *EuroIntervention* 2007 November;3(3):365-70.

(11) Gutierrez-Chico JL, Cortes C, Schincariol M, Jaguszewski M. A formula to calculate the contrast volume required for optimal imaging quality in optical coherence tomography with non-occlusive technique. *Cardiol J* 2018;25(5):574-81.

(12) Prabhu S, Schikorr T, Mahmoud T, Jacobs J, Potgieter A, Simonton C. Engineering assessment of the longitudinal compression behaviour of contemporary coronary stents. *EuroIntervention* 2012 June 20;8(2):275-81.

(13) Tomberli B, Mattesini A, Baldereschi GI, Di MC. A Brief History of Coronary Artery Stents. *Rev Esp Cardiol (Engl Ed)* 2018 May;71(5):312-9.

(14) Barkholt TO, Webber B, Holm NR, Ormiston JA. Mechanical properties of the drug-eluting bioresorbable magnesium scaffold compared with polymeric scaffolds and a permanent metallic drug-eluting stent. *Catheter Cardiovasc Interv* 2019 November 11.

(15) Silber S, Gutiérrez-Chico JL, Behrens S, Witzenbichler B, Wiemer M, Hoffmann S, Slagboom T, Harald D, Suryapranata H, Nienaber C, Chevalier B, Serruys PW. Effect of paclitaxel elution from reservoirs with bioabsorbable polymer compared to a bare metal stent for the elective percutaneous treatment of de novo coronary stenosis: the EUROSTAR-II randomised clinical trial. *EuroIntervention* 2011 May;7(1):64-73.

(16) Virmani R, Guagliumi G, Farb A, Musumeci G, Grieco N, Motta T, Mihalcsik L, Tespili M, Valsecchi O, Kolodgie FD. Localized Hypersensitivity and Late Coronary Thrombosis Secondary to a Sirolimus-Eluting Stent: Should We Be Cautious? *Circulation* 2004 February 17;109(6):701-5.

(17) Gutierrez-Chico JL, Jaguszewski M, Comesana-Hermo M, Correa-Duarte MA, Marinas-Pardo L, Hermida-Prieto M. Macrophagic enhancement in optical coherence

tomography imaging by means of superparamagnetic iron oxide nanoparticles. *Cardiol J* 2017 May 12.

(18) Wu P, Gutiérrez-Chico JL, Tauzin H, Yang W, Li Y, Yu W, Chu M, Guillon B, Bai J, Meneveau N, Wijns W, Tu S. Automatic stent reconstruction in optical coherence tomography based on a deep convolutional model. *Biomed Opt Express* 2020;11(6):3374-94.

Figure legends

Figure 1: Nomenclature of the stent platform for the current study.

The two fundamental components were sinusoidal hoops and the longitudinal connectors. Peaks and valleys were defined in the hoops as if the proximal part of the vessel were the earth and the distal part were the sky (panel A). Hinge points with the vertex pointing to the distal part were peaks, while hinge points with the vertex pointing to the proximal part were valleys. The struts between peaks and valleys were dubbed slopes. The terms upslope and downslope were defined according to a consistent direction (for instance left to right) at the analyst's discretion. Panel B shows the OCT view, with the distal part at the left part of the screen.

Figure 2: Nomenclature of longitudinal connectors for the current study.

Longitudinal connectors (or direct connections) peak-to-peak, peak-to-valley and valley-to-valley. .

Figure 3: Design and OCT examples of the different stent platforms in the study.

Figure 4: Paradigmatic case of a restenosis (A) in a Biodivysio stent (B), (Biocompatibles Ltd, Farnham, UK), showing the 4 steps of the protocol.

Step 1: 3D view with automatic detection of struts.

Step 2: 3D direct tissue view, without automatic detection of struts.

Step 3: Longitudinal view with automatic detection of struts.

Step 4: 3D view in mode "stent only".

Figure 5: Study flow-chart.

NURD: Non-uniform rotational distortion; OCT: Optical coherence tomography

Figure 6: Diagnostic efficiency of each step of the protocol, stratified by timing of the stent implant and by pullback speed.

Figure 7: Combination of steps in which the stent is recognised, stratified by timing of the stent implant and by pullback speed.

Tables

Table 1: Descriptive statistics of patients, intervention and lesions.

Patient level	**n = 146**
Male (%)	112 (76.7)
Age, years	66.0 (59.0 – 75.2)
BMI (SD)	28.1 (4.8)
CV risk factors:	
- Hypertension	118 (80.8)
- Hypercholesterolemia	70 (47.9)
- Diabetes mellitus	
▪ Type 2 on OAD	41 (28.1)
▪ Type 2 insulin-requiring	12 (8.2)
- Smoking	
▪ Previous smoker	28 (19.2)
▪ Current smoker	34 (23.3)
- Family history of CHD	7 (4.8)
Previous MI	54 (37.0)
Previous revascularisation	
- PCI	81 (55.5)
- CABG	9 (6.2)
GFR (Cockroft-Gault), ml/min	86.8 (45.3)
Serum Haemoglobin, g/dl	13.5 (1.7)
LVEF, %	60 (12)
Procedural variables:	**n = 155**
Syntax score	13.7 (8.6)
Contrast volume, ml	232 (106)
Fluoroscopy time, min	20.8 (15.8)
Clinical indication	
- Stable coronary disease	108 (69.7)
- Unstable angina	22 (14.2)
- Non-ST- elevation MI	22 (14.2)
- ST-elevation MI	3 (1.9)
Lesions	**n = 179**
Calcification	
- None to little	155 (86.6)
- Moderate to severe	24 (13.4)
DS, %	72.5 (15.9)

BMI: body mass index; CABG: coronary artery bypass graft; CHD: coronary heart disease; CV: cardiovascular; DS: diameter stenosis; GFR: glomerular filtration rate; LVEF: left ventricular ejection fraction; MI: myocardial infarction; OAD: oral antidiabetics; PCI: percutaneous coronary intervention.

Data presented as counts (percent), mean (standard deviation) or median (P_{25} – P_{75}).

Table 2: Descriptive statistics of the analysed stents.

Stents analysed	**n = 294**
Coronary artery	
- Left main	11 (3.7)
- Left anterior descending	123 (41.8)
- Diagonal	12 (4.1)
- Circumflex	45 (15.3)
- Obtuse marginal	10 (3.4)
- Right coronary artery	91 (31.0)
- Posterolateral	2 (0.7)
Type of stent implanted	
- Xience	69 (23.5)
- Magmaris	55 (18.7)
- Biofreedom	23 (7.8)
- Firebird	22 (7.5)
- Resolute Integrity	19 (6.5)
- Orsiro	17 (5.8)
- Coroflex	14 (4.8)
- Promus Element	12 (4.1)
- Bioss-Lim C	10 (3.4)
- ML Rx Pixel	9 (3.1)
- Firehawk	9 (3.1)
- Resolute Onyx	7 (2.4)
- Driver	6 (2.0)
- Taxus Liberté	4 (1.4)
- Nobori	4 (1.4)
- Biomatrix	3 (1.0)
- ML Zeta	2 (0.7)
- Vision	2 (0.7)
- Biodivysio	2 (0.7)
- Alex Plus	2 (0.7)
- Cypher	1 (0.3)
- Taxus Express	1 (0.3)
- Costar	1 (0.3)
Timing of implant	
- Recently implanted (<3 months)	187 (63.6)
- Late implanted (≥3 months)	107 (36.4)
Immediately post-implant	160 (54.4)
Time from stent implantation (months) *	23.9 (8.7 – 61.6)
In-stent restenosis	62 (21.1)
Mehran's type §	
- Ia	1 (1.6)
- Ib	3 (4.8)
- Ic	11 (17.7)

- Id - II - III - IV	0 (0.0) 27 (43.6) 18 (29.0) 2 (3.2)
Overlap	132 (44.9)
Pullback speed	
- 18 mm/s - 36 mm/s	227 (77.2) 67 (22.8)

LVEF: left ventricular ejection fraction

Data presented as counts (percent) or median (P_{25} – P_{75}).

* For the group of late implanted stents.

§ For the subgroup with in-stent restenosis.

Table 3: Agreement between the stent platform identified by the analysts and the platform implanted.

	Kappa	95% CI		p-value
		Lower	Upper	
Agreement with implanted stent platform	0.965	0.943	0.987	<0.0001
- Recently implanted (<3 months)	0.993 (0.006)	0.981	1.000	<0.0001
- Late implanted (≥ 3 months)	0.915 (0.028)	0.860	0.970	<0.0001
- ISR	0.889 (0.042)	0.807	0.971	<0.0001
- PB speed 18 mm/s	0.969 (0.013)	0.944	0.994	<0.0001
- PB speed 36 mm/s	0.940 (0.033)	0.875	1.000	<0.0001
Interobserver agreement	0.988	0.974	1.000	<0.0001

CI: Confidence interval; ISR: In-stent restenosis; PB: Pullback

Table 4: Efficiency of each step to recognise the stent.

	Recently implanted	Late implanted
PB speed 18 mm/s	144	83
- Step 1: 3D with automatic strut	127 (88.2)	70 (84.3)
- Step 2: 3D tissue	144 (100.0)	65 (78.3)
- Step 3: Longitudinal view	131 (91.0)	75 (90.4)
- Step 4: 3D stent only	127 (88.2)	66 (79.5)
PB speed 36 mm/s	43	24
- Step 1: 3D with automatic strut	32 (74.4)	16 (66.7)
- Step 2: 3D tissue	42 (97.7)	14 (58.3)
- Step 3: Longitudinal view	41 (95.3)	22 (91.7)
- Step 4: 3D stent only	32 (74.4)	14 (58.3)
Step 1	159 (85.0)	86 (80.4)
Step 2	186 (99.5)	79 (73.8)
Step 3	172 (92.0)	97 (90.7)
Step 4	159 (85.0)	80 (74.8)
Combination of steps	187	107
- Unrecognisable	1 (0.5)	7 (6.5)
- Step 1 only	0 (0.0)	0 (0.0)
- Step 2 only	14 (7.5)	3 (2.8)
- Step 3 only	0 (0.0)	5 (4.7)
- Step 4 only	0 (0.0)	0 (0.0)
- Steps 1+2	0 (0.0)	0 (0.0)
- Steps 1+3	0 (0.0)	2 (1.9)
- Steps 1+4	0 (0.0)	0 (0.0)
- Steps 2+3	13 (7.0)	5 (4.7)
- Steps 2+4	0 (0.0)	0 (0.0)
- Steps 3+4	0 (0.0)	0 (0.0)
- Steps 1+2+3	0 (0.0)	5 (4.7)
- Steps 1+2+4	0 (0.0)	0 (0.0)
- Steps 1+3+4	0 (0.0)	14 (13.1)
- Steps 2+3+4	0 (0.0)	1 (0.9)
- All the steps	159 (85.0)	65 (60.7)

Data presented as count (percent) of stents that were correctly identified.

PB: Pullback

Figure 1

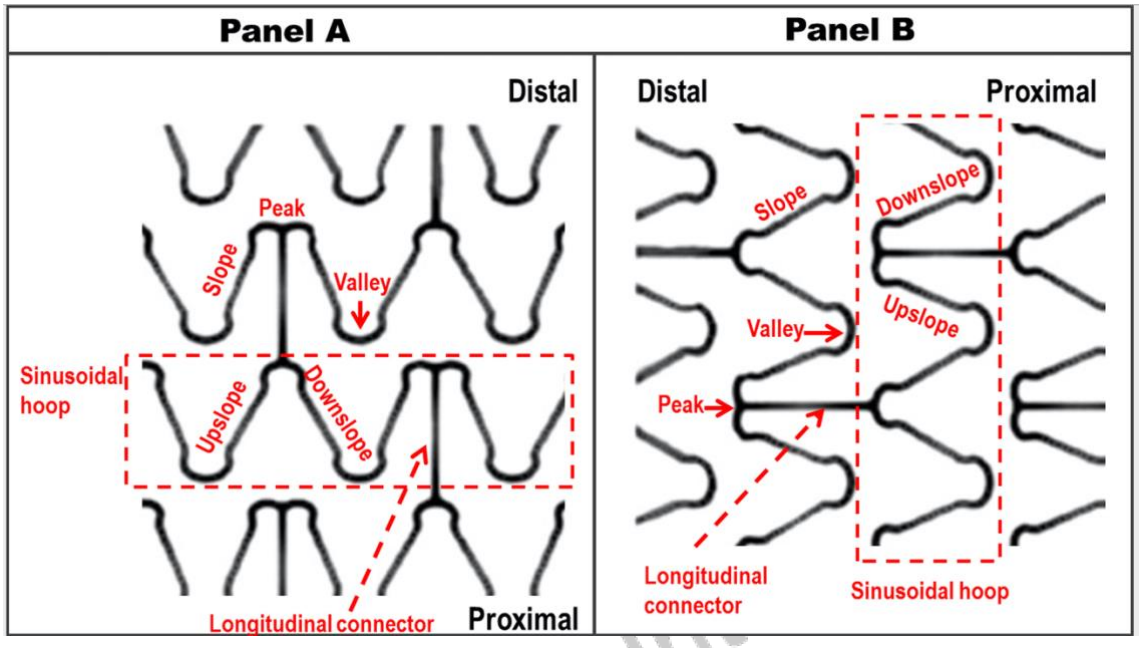

Figure 2

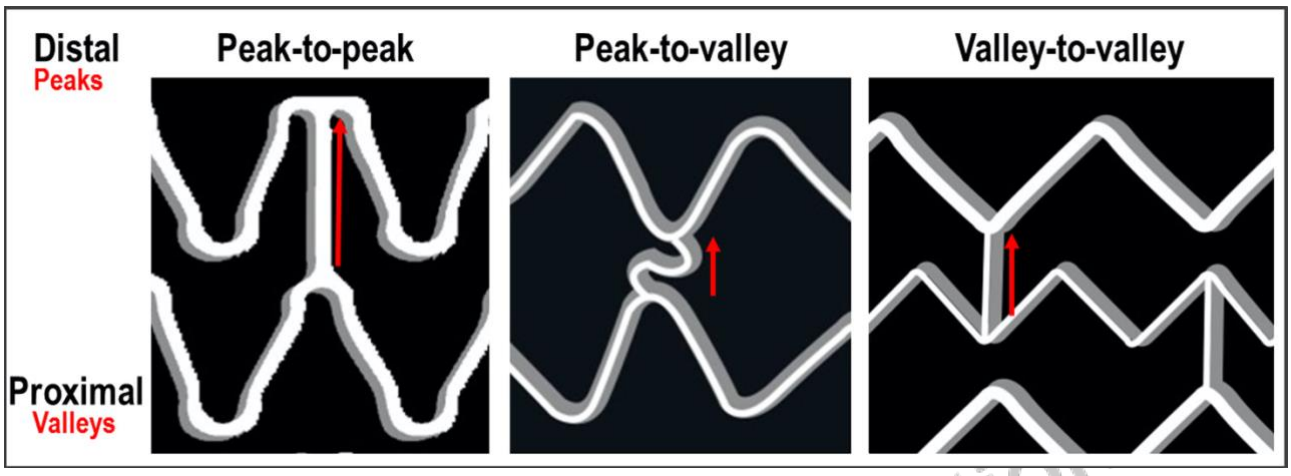

Figure 3 panel 1

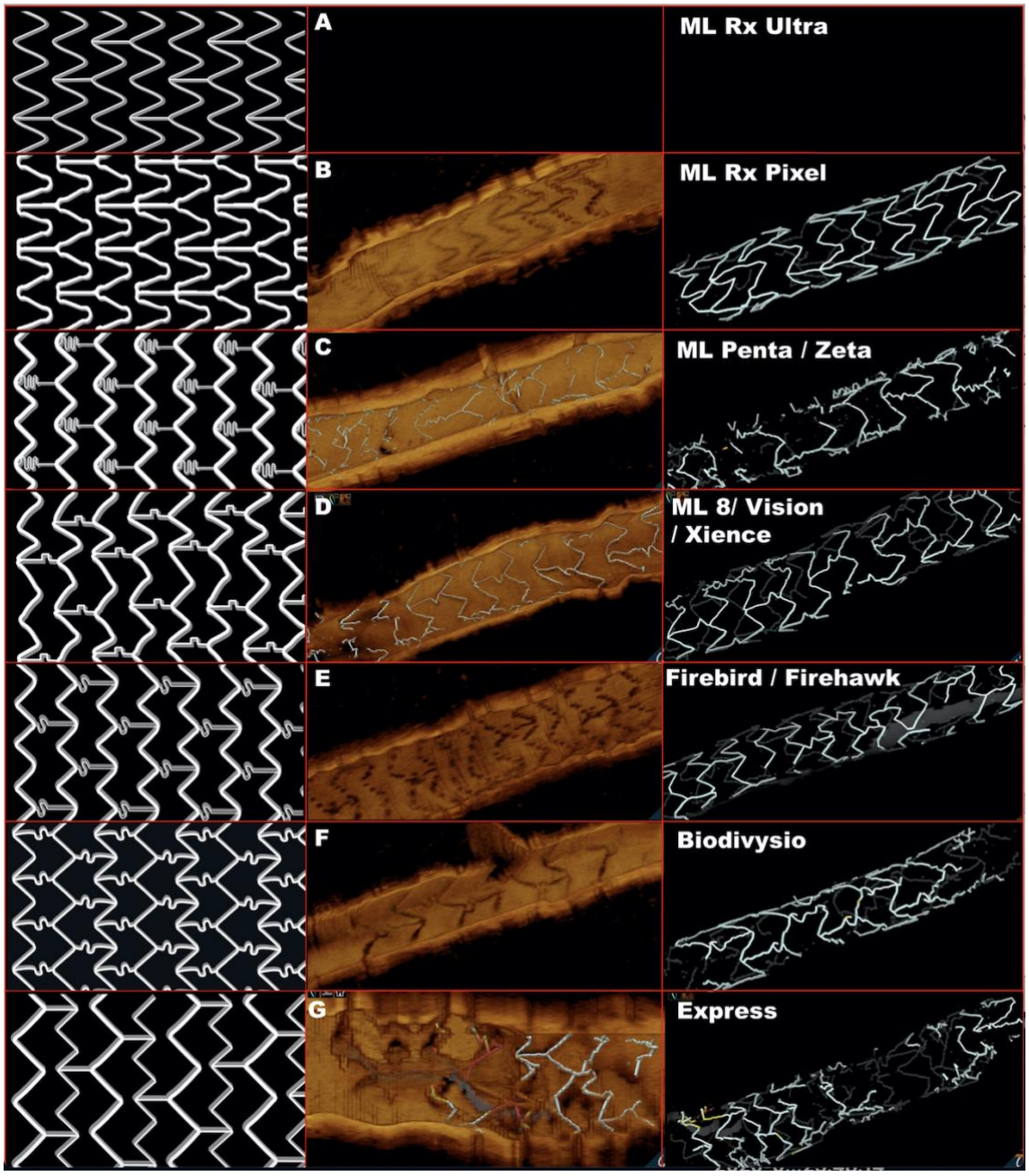

Figure 3 panel 2

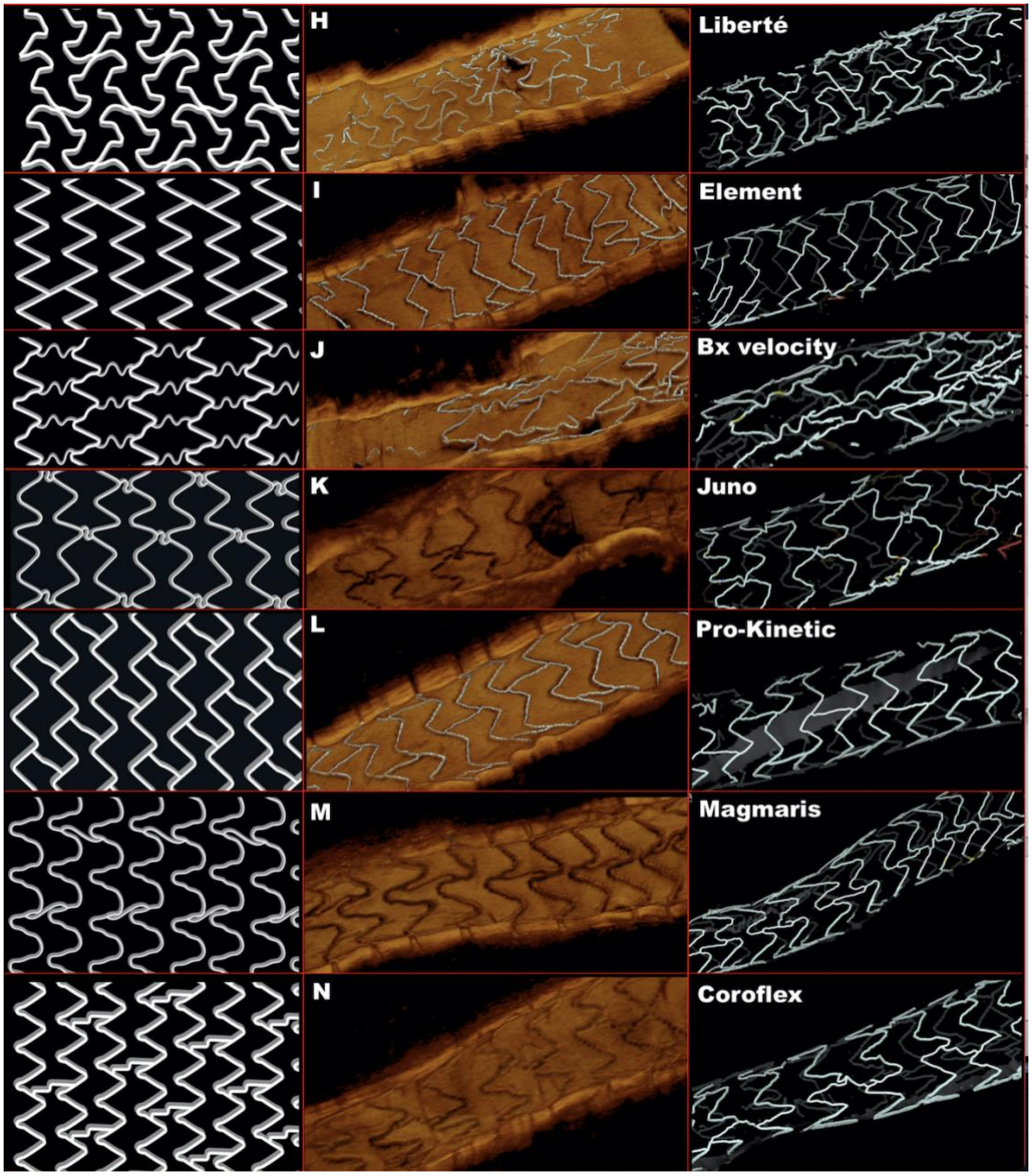

Figure 3 panel 3

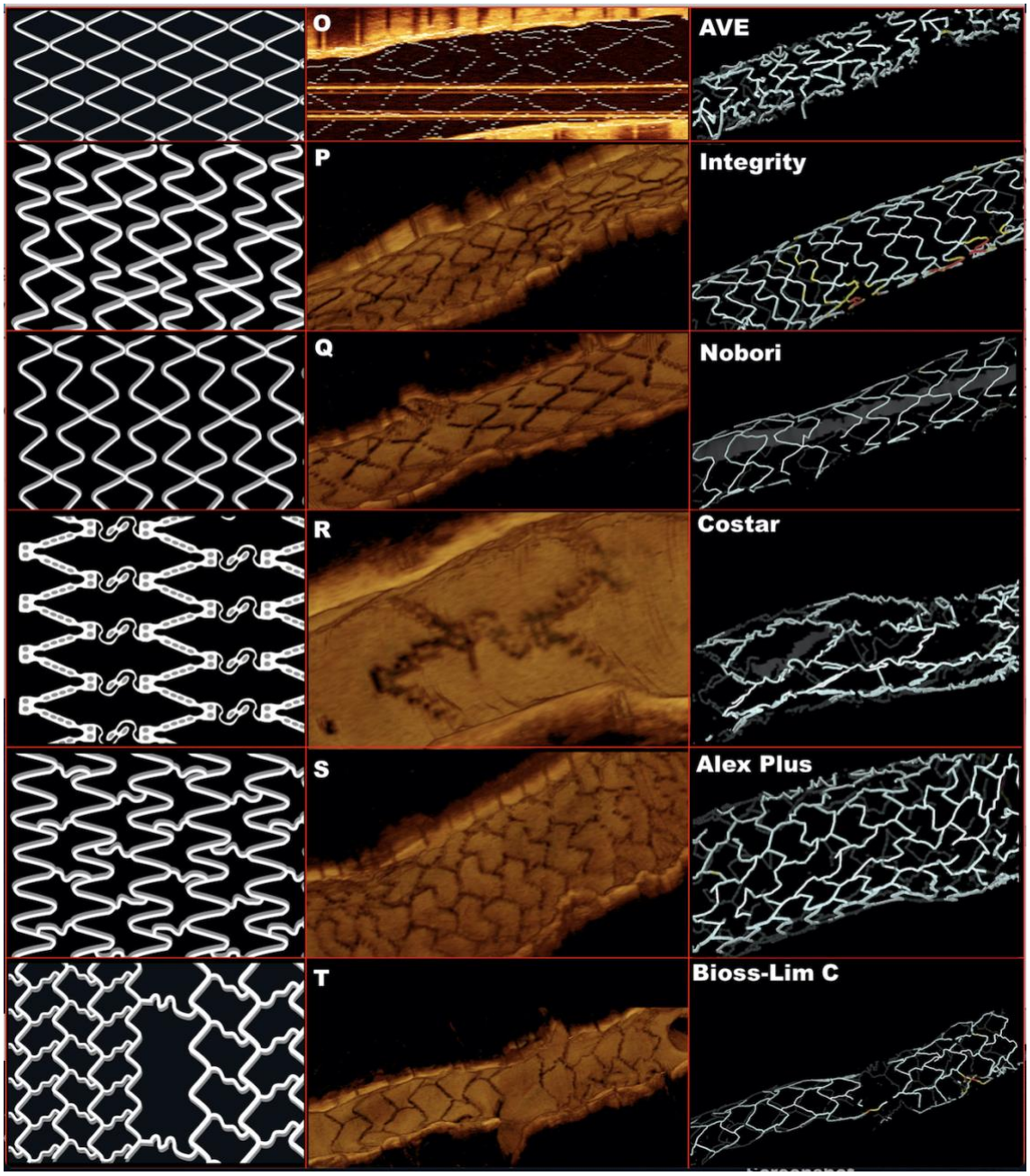

Figure 4

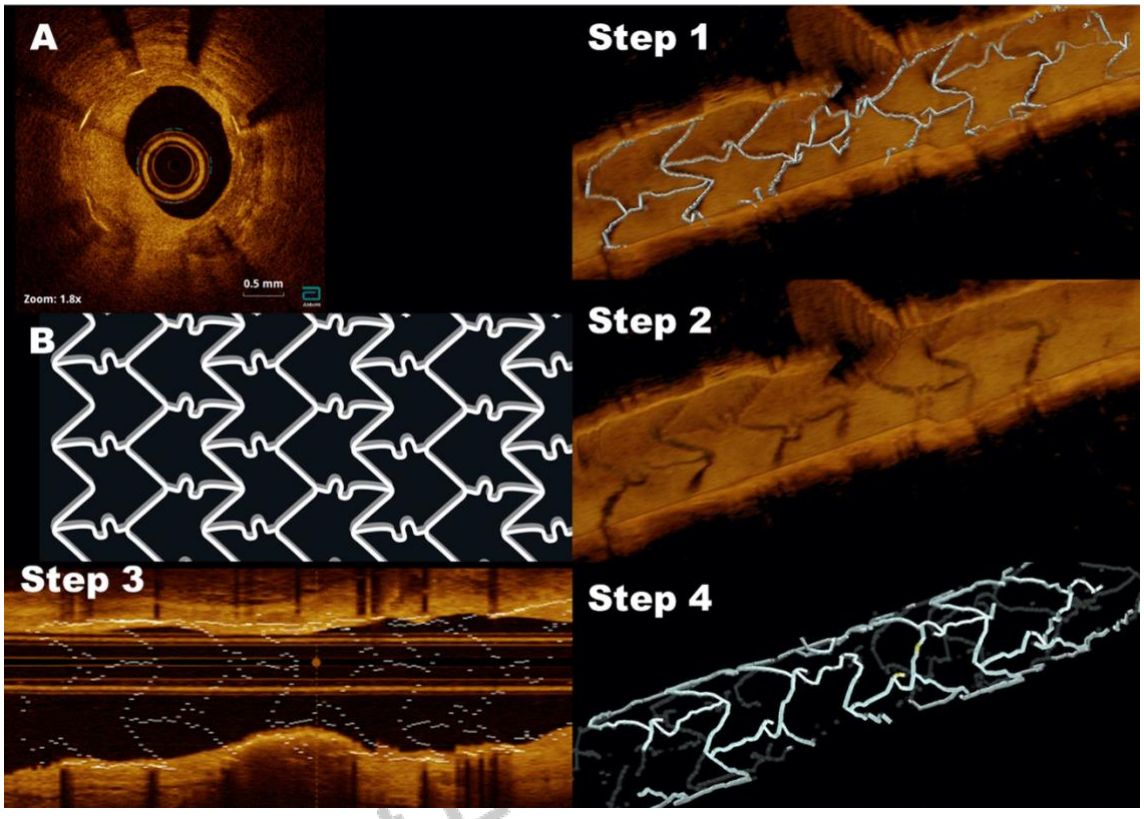

Figure 5

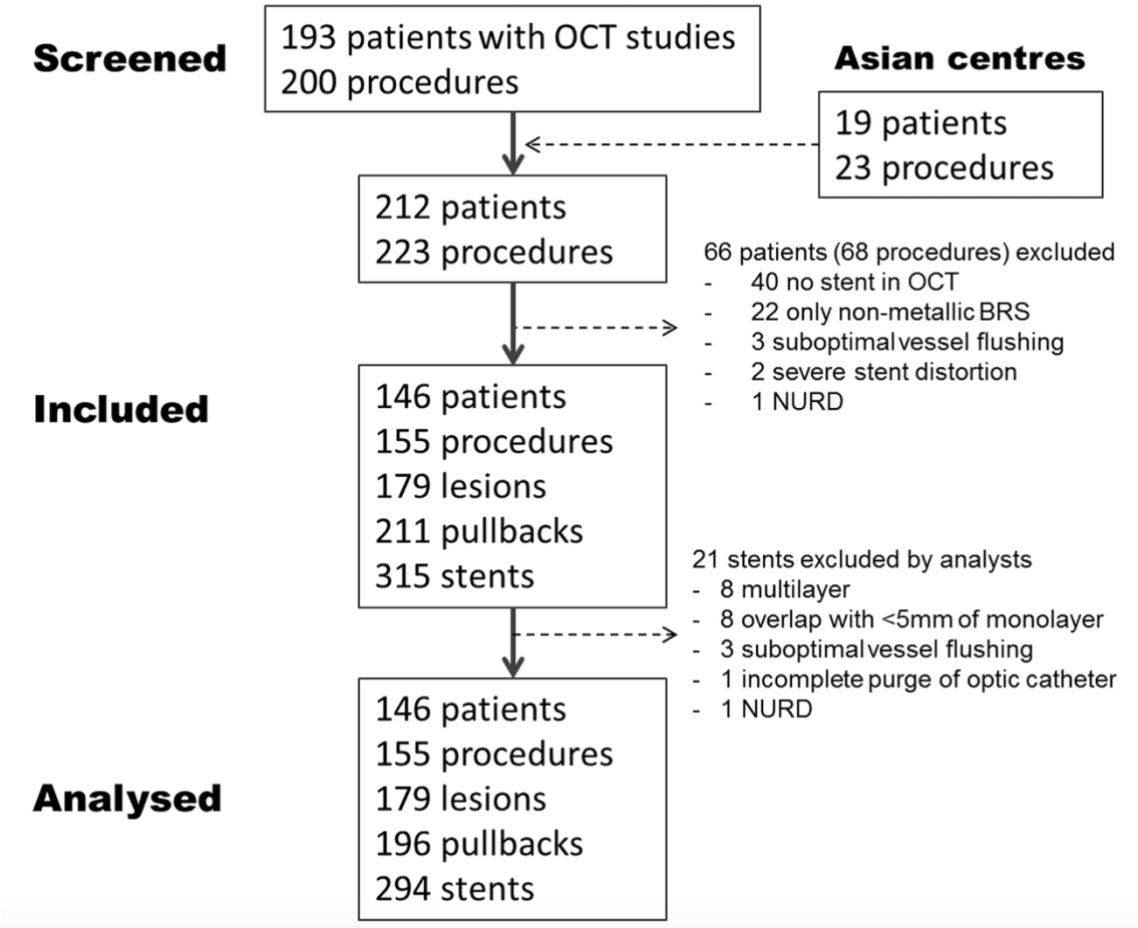

Figure 6

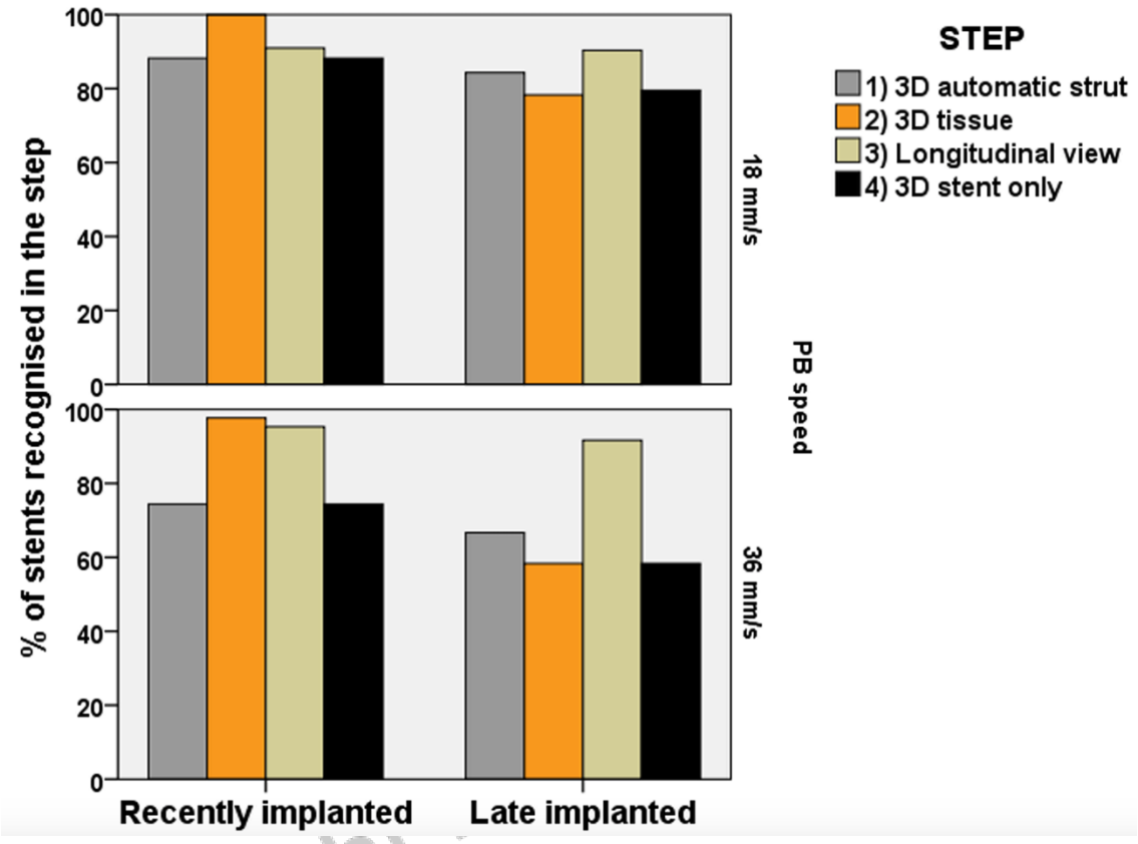

Figure 7

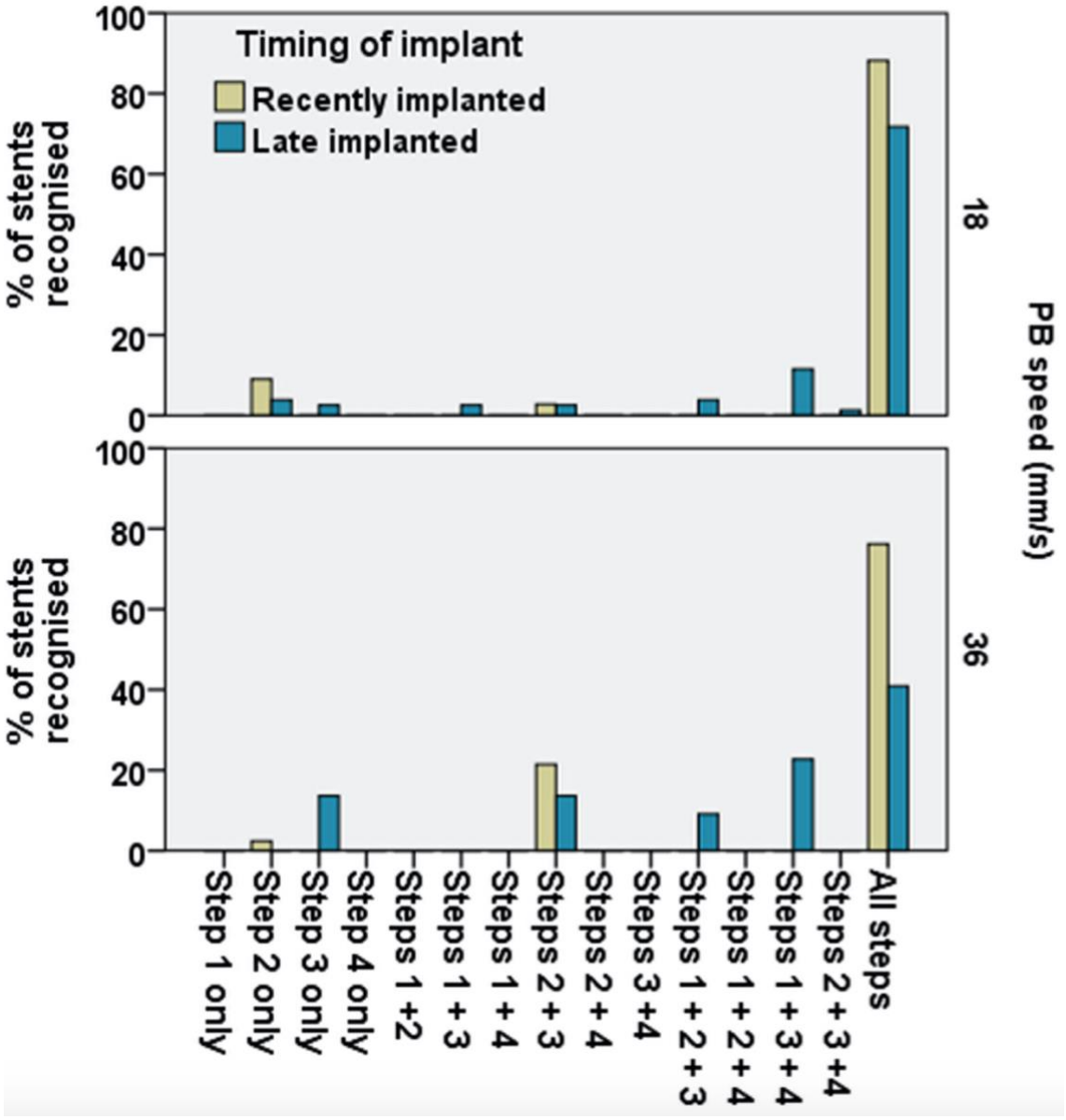

Tables

Supplementary table 1: Definition of the different stent patterns

Stent platform	Sinusoidal hoops	Longitudinal connector	Model and OCT
MultiLink Rx Ultra	In-phase	• Peak-to-peak • Straight • Linking 2 adjacent hoops.	Figure 3, panel 1A
MultiLink Rx Pixel	In-phase	• Peak-to-peak • Straight • Linking 3 consecutive hoops, alternating with connectors linking only 2 adjacent hoops	Figure 3, panel 1B
MultiLink Penta / Zeta	In-phase	• Peak-to-peak • Sinusoidal ACCESS connectors, consisting of 5 turns (2 peaks at each side of the connector)	Figure 3, panel 1C
MultiLink 8 / Vision platform (Xience)	In-phase	• Peak-to-peak • Typical crenelated shape	Figure 3, panel 1D
Firebird / Firehawk	In-phase	• Valley-to valley or peak-to-peak (one design or the other) • S-shaped connector at the obtuse angle, (3 turns, one peak at each side of the connector) • Last hoop at proximal and distal extremes are connected by peak-to-valley S-shaped connector	Figure 3, panel 1E
Biodivysio	In-phase	• Peak-to-peak, alternating with • Valley-to-valley in the adjacent rings • S-shaped connector at the inferior peak or upper valley, (3 turns, one peak at each side of the connector)	Figure 3, panel 1F
Express platform (Taxus)	Sinusoidal hoops, alternating different frequencies (wide hoops with long struts and few peaks, narrow hoops with short struts and more peaks), thus appearing as in-phase or out-of-phase at different points	• Peak-to-peak, alternating with • Valley-to-valley in the adjacent rings	Figure 3, panel 1G
Liberté platform (Taxus)	In-phase, with asymmetrical and tilted peaks/valleys, giving a	• Direct peak-to-valley connection, possible due to the asymmetry and tilt of the design	Figure 3, panel 2H

	typical interdigitated appearance		
Element platform (Taxus / Promus / Synergy)	Offset (Almost out-of-phase)	• Peak-to-valley • Short straight connector, aligned with the direction of the slope	Figure 3, panel 2I
Bx-Velocity platform (Cypher)	Out-of-phase	• Sinusoidal longitudinal connector • Connecting the slopes, (almost peak-to-valley)	Figure 3, panel 2J
Juno Platform (Biomatrix)	Out-of-phase	• Peak-to-valley • S-shaped connector	Figure 3, panel 2K
Pro-Kinetic platform (Orsiro)	Offset	• Mid-points of the slopes • Semi-straight connector • From upslope to upslope • Perpendicular to the slopes	Figure 3, panel 2L
Magmaris	Offset	• Mid-points of the slopes • Sinusoidal connector • From upslope to upslope • Parallel to the slopes	Figure 3, panel 2M
Coroflex	Offset	• Mid-points of the slopes • Typical step-shaped connector • From downslope to upslope (coroflex blue) or slopes of the same kind (coroflex ISAR neo).	Figure 3, panel 2N
AVE platform (Driver, Endeavor, Resolute)	Out-of-phase	• Direct peak-to-valley connection • By welds • Regular structure	Figure 3, panel 3O
Integrity and Onyx platforms (Resolute)	Out-of-phase Irregular alignment (single wire)	• Direct peak-to-valley connection • By welds • Connection every 4 peaks • Irregular structure	Figure 3, panel 3P
Nobori	Out-of-phase Regular alignment	• Direct peak-to-valley connection • By welds • Connection every 3 peaks • Regular structure	Figure 3, panel 3Q
Costar	Out-of-phase Typical strut appearance with wells along the struts	• Peak-to-valley • Sinusoidal connector with wells	Figure 3, panel 3R
Alex plus	In-phase	• Peak-to-slope, alternating with • Valley-to-slope in the adjacent rings	Figure 3, panel 3S
Bioss-Lim C	In-phase Two differentiated segments linked by 2 longitudinal connectors	• Peak-to-slope	Figure 3, panel 3T

2**Supplementary table 2:** Summary of the technical requirements for each step of the protocol.

Step	**Dimensions**	**ASD**	**Post-processing**
1: 3D + ASD	3D	Yes	Yes
2: 3D tissue view	3D	No	No
3: Longitudinal view	2D	Yes	No
4: Stent only	3D	Yes	Yes

ASD: Automatic strut detection